

Revisiting galaxy rotation curves using a non-parametric regression method

Lizbeth M. Fernández-Hernández,^{1§*} Ariadna Montiel^{2†*}, Mario A. Rodríguez-Meza^{1‡*}

¹Departamento de Física, Instituto Nacional de Investigaciones Nucleares, AP 18-1027, Ciudad de México 11801, México

²Instituto de Ciencias Físicas, Universidad Nacional Autónoma de México, 62210, Cuernavaca, Morelos, México*
(Dated: December 15, 2024)

So far several density profiles have been proposed to explain the contribution of dark matter (DM) halos to rotation curves of galaxies. In this work, without any assumption about the dynamics of the system, we apply a non-parametric method to reproduce the rotation curves of SPARC galaxies for a set of models type Core, Cusp and Core+Cusp (Fuzzy) which are the Pseudo Isothermal (Piso), NFW, Burkert, Spano, Schive, the soliton+NFW profile in the Fuzzy DM (FDM) model with one continuity condition on the density profile (SNFWC) and with two continuity conditions on the density profile and on the first derivative of the density (SNFWDC). A comparison of the rotation curve obtained using the non-parametric reconstruction method with the one obtained using the standard model fitting method, is performed by computing the distance between central curves (B_{DIST}) and the distance between 1σ errors bands ($B_{D1\sigma}$). Besides, with statistics tools such as P -value, BIC, AIC, χ^2_{red} we do a model selection according with best values. Therefore, to do a model selection we establish three conditions as a criterion to accept or reject models: the best BIC value; the lowest B_{DIST} value and the lowest $B_{D1\sigma}$ value. We work with two groups of models. The first one is a comparison between Core and Cusp models (Piso, NFW, Spano and Burkert) and we show that Spano is the most favored model satisfying the above three conditions with the 60.87%. For the second group we select Core, Cusp and Fuzzy models (Schive, NFW, SNFWDC, SNFWC), finding that Schive model is in agreement in 43.75% with the above established conditions. Moreover according with the statistical tools and non-parametric reconstruction we are able to classify some of the galaxies as Core or Cusp.

I. INTRODUCTION

One of the main problems to solve in galactic dynamics is to determine the role of the DM halo whose first manifestation was observed in the measured rotation curves[1]. In the literature we can find a considerable amount of density profiles trying to explain the contribution of dark matter halos to the rotation curves (Burkert, Pseudo Isothermal, Spano, Einasto, Gaussian, Schive, to mention just a few profiles)[2–8]. Some of them have been obtained from N -body simulations of structure formation. These simulations can reproduce most of the characteristics of the universe at galactic scales, but not at smaller ones such as dwarf galaxies or satellite galaxies. This characteristics can be attributed to the importance of the baryonic part in the dynamics of structure formation. On the other hand, the cusp-core problem is manifested in the rotation curves of some galaxies where in the center of the dark matter halo has a core behavior $\rho_{DM} \sim \text{constant}$, which is in disagreement with the cuspy behavior predicted by the simulations, $\rho_{DM} \sim r^{-1}$. Furthermore, Schive *et al.* [9] obtained a density profile from a cosmological simulation which has an inner

soliton-like profile (SFDM) and the asymptotic NFW decline in the outer points, called Fuzzy, wave or ultra-light axion DM[10].

Each density profile or model of rotation curves assumes a specific functional behavior in the configuration space being the parameters of the theory constrained or determined by observational data using fitting data analysis like minimizing the χ^2 or by using bayesian methods like Monte Carlo-Markov Chain method. In contrast, it is possible to obtain model independent information directly from observations using non-parametric methods [11–17]. In the latter scenario, it is assumed a correlation between each data point but is not required prior information about the functional form of the observable. Even more these techniques are very useful for building and checking parametric models, as well as for data description.

In this work, we use a powerful but simple non-parametric regression technique called Locally Weighted Scatterplot Smoothing (Loess) method originally introduced in [18] and further developed in [19] to reconstruct rotation curves of galaxies without assuming any prior or DM model. Loess recovers the global trend of data by using a weighted least squares by fitting a low-degree polynomial to a subset of the data, giving more weight to points near the point whose response is being estimated and less weight to points further away. Further, to take into account the measurement errors of data, we use the Simulation and Extrapolation method (Simex) [20, 21]. These methods were proposed to use them together in Cosmology in [22] obtaining a suitable success. Later,

* Part of the Instituto Avanzado de Cosmología (IAC) Collaboration

§ E-mail:lfernandez@fis.cinvestav.mx

† E-mail:amontiel@icf.unam.mx

‡ E-mail:marioalberto.rodriguez@inin.gob.mx

this technique was applied to reconstruct other cosmological quantities in [23–25] showing also good results.

Here we are primarily dedicated to study the influence of the galactic DM halo on the rotation curves applying the Loess+Simex method, for which we use a selection of galaxies from SPARC (Spitzer Photometry and Accurate Rotation Curves) [26], whose main feature is that the contribution of dark matter is greater than 50% such that the structure of the rotation curve comes mostly from dark matter and not from baryonic information (gas and stars). We also perform a comparison of the χ^2 fitted velocity rotation curves with the non-parametric reconstruction method through the distance between central curves (B_{DIST}) and the distance between 1σ errors bands ($B_{D1\sigma}$). Besides, in our analysis we use statistics tools such as P -value, Bayesian information criterion (BIC), Akaike information criterion (AIC) and minimizing the reduced χ^2 in order to do a model selection according with the best values. In particular we work with two groups of models. The first one is aimed to compare between Core and Cusp models (Piso, NFW, Spano and Burkert) and the second group is aimed to compare Core, Cuspy, and Fuzzy models (Schive, NFW, SNFWDC, SNFWC). Therefore, to do a model selection among the groups we establish three conditions as a criteria to accept or reject models: the best BIC value; the lowest B_{DIST} value and the lowest $B_{D1\sigma}$ value. Additionally, from the statistical tools mentioned before and the non-parametric reconstruction, we investigate a possible classification of galaxies as core or cuspy.

The structure of this work is as follows: in Sec. II we review the main idea behind the galaxies rotation curves and how was done the selection of galaxies from SPARC which we have worked with; in Sec. III we briefly summarize the Loess and Simex techniques; in Sec. IV, we present the statistical methodology to perform the model selection; in Sec. V we report and discuss our results and finally we end up with the conclusions in Sec. VI.

II. GALAXY ROTATION CURVES

Let us start by pointing out that we study rotation curves of galaxies within the weak gravitational field limit in order to investigate DM parameters.

The rotation curve is obtained from the absolute value of the effective gravitational force as:

$$\begin{aligned} V^2(r) &= r \left| \frac{d\Phi(r)}{dr} \right| \\ &= \sqrt{G \frac{M_{DM}(r)}{r} + \Upsilon_{Disk} V_{Disk}^2 + V_{Gas}^2}, \end{aligned} \quad (1)$$

where $\Phi(r)$ is the gravitational potential, $M_{DM}(r)$ is the mass halo for a DM distribution, V_{Disk} and V_{Gas} are the contributions of the stellar disk and gas disk velocities and Υ_{Disk} is the stellar mass-to-light ratio of disk.

The models we select to fit each rotation curve can be reviewed in the appendix A; there we show the explicit

form of the density profile and the velocity function in every case we considered in this work.

Regarding the galaxy selection we are considering the baryonic contribution for each rotation curve (Disk and Gas), $\Upsilon_{Disk} = 0.5 M_{\odot}/L_{\odot}$ at [3.6] and $\Upsilon_{Gas} = 1.33 M_{\odot}/L_{\odot}$ ([26–28]).

On the other hand, in order to allow that the dark matter has a considerable contribution in the fit, we choose galaxies from SPARC where the percentage of dark matter meets $90 > \%DM > 60$ with $\%DM = (M_{DM}(r_{max}) * 100) / (M_{Bar}(r_{max}) + M_{DM}(r_{max}))$, M_{DM} corresponds to the dark matter mass contribution for each model and M_{Bar} to the total baryonic mass, both of them evaluated at the outer measured radius value of the rotation curve observational data (r_{max}).

With this selection of galaxies and using the values of the mass at the outer observed radius, we can classify them according to the dominant baryonic component, consequently, those dominated by gas are of the order of 83.3%, dominated by the stellar disk, 14.6% and 2.08% where the gas and the stellar disk contribute with the 50% from the total photometric information (NGC 0300, for example). However, according to the morphology of the galaxies and the Hubble classification, we have a galaxy selection where $\sim 33.3\%$ are Sm, 27.08% Im, 20.83% Sd, Scd = Sdm = 6.25%, 4.17% Sc and 2.08% BCD [26].

III. NON-PARAMETRIC RECONSTRUCTION METHOD

Recently, in [22] has been introduced a non-parametric reconstruction method based on Loess and a simple simulation algorithm that allows to display the effect of measurement errors on parameter estimates, Simex. In this section, we briefly review the main features of Loess and Simex.

1. Basis of Loess

Loess is a non-parametric method in the sense that the fitting is performed without having to specify in advance the relationship between the dependent and independent variables. At each point of the data set a low-degree polynomial is fit to a subset of this data, the polynomial is obtained by weighted least squares, giving more weight to points near to the point whose response is being estimated and less weight to points further away. The value of the regression function for the point is then obtained by evaluating the local polynomial using the independent variable value for that data point. The Loess fit is complete after regression function values have been computed for each of the n observational measurements. This whole process offers the possibility to get the full view of the global trend of the data, which is the original objective of the procedure. To obtain the graphical account of the re-

relationship between dependent and independent variables, it is just required to join the reconstructed points with a line.

Here we work with observational data of rotation curves of galaxies, so that the radius or distance from the center of the galaxy, R , measured in kpc is our independent variable and the velocity, V , of the stars or gas particles of the galaxy in units of km/s, corresponds to the dependent variable.

In the following the main features of the method are briefly discussed. For further details we encourage the reader to see [22] and references therein.

i. *Smoothing Parameter*

The *smoothing parameter*, s , also called *span* determines how many data points should be used in each weighted least squares fit. The *span* ranges between 0 and 1 and controls the flexibility of the *Loess* regression function. Large values of s produce the smoothest functions that wiggle the least in response to fluctuations in the data but small values of s produce more irregular reconstructed curves, because the intrinsic noise and dispersion of data is fully captured. As in [22], the election of the optimal value of the *span* s is done by using the *cross-validation* method.

ii. *Weight Function*

As mentioned above, the weight function gives the most weight to the data points nearest the point of estimation and the least weight to the data points that are furthest away.

The traditional weight function used for Loess is the tri-cube weight function,

$$w(x) = \begin{cases} (1 - |x|^3)^3 & \text{for } |x| < 1 \\ 0 & \text{for } |x| \geq 1 \end{cases}. \quad (2)$$

However, any other weight function that satisfies the properties listed in [18] could also be used. Between the properties needed are that the weight function should be positive and that the treatment to the points to the left of x_i is not be different from those to the right. In addition, it is desirable that $w(x)$ decrease smoothly to 0 as x goes from 0 to 1. Among the weight functions that decrease to 0, normally the tricube function is chosen since provides an adequate smooth in almost all situations. Here, as in [22], this weight function is used.

iii. *Degree of Local Polynomials*

The idea behind Loess is to fit each subset of data using polynomials of a low degree after the weight function is applied. The polynomials are almost always of first or second degree and although higher-degree polynomials would work, it could cause overfit the data in each subset besides of higher computational cost without giving any significant improvement in the result.

iv. *Confidence regions*

To construct the confidence regions of the nonparametric regression, it is made an analogy with the standard least squares regression by using the local polynomial estimate, that results from the locally weighted least-squares regression of y on the x values in each chosen window, and by assuming normally distributed errors. In this way, the 68%-percent confidence interval and the 95%-percent confidence interval of the regression function can be constructed. For many more details see [22, 29] and references therein.

2. *Basis of Simex*

Simex is a simple simulation and extrapolation algorithm that allows to display the effect of measurement errors on parameter estimates, firstly proposed in [20, 21].

Since the observational errors are not contemplated by Loess method, in [22] was suggested to use these two methods together as a valuable technique for visualizing complex relationships between cosmological quantities.

Basically Simex works as follows:

- i. The method starts with the *simulation step* in which some additional error is added in each observation y_i in the data set, with $i = 1, \dots, n$ and n the number of data points, following the rule

$$\eta_i(\lambda) = y_i + \sqrt{\lambda}\sigma_i, \quad \lambda > 0 \quad (3)$$

where σ_i is the measurement error variance associated to the observed data y_i and the parameter λ acts as the controlling parameter for the amount added of σ_i . We take, as in [22], $\lambda = \{0.5, 0.6, 0.7, \dots, 2.0\}$ to simulate the *new* datasets.

- ii. The last stage is the *extrapolation step*. After introducing the variable λ , the final measurement error variance associated with the simulated data points, $\eta_i(\lambda)$, is $(1 + \lambda)\sigma_i^2$. So, it is necessary to take $\lambda \rightarrow -1$, in order to return back to the original data without uncertainties and to trace the effect of the measured error in the original data. This is done via a regression analysis, using a quadratic polynomial, on the *new* datasets.

Up to this point, we have addressed briefly the features and free parameters of *Loess+Simex* method, however many more details of it can be found in Refs. [20–22, 29–35] and references therein.

IV. PARAMETRIC STATISTICAL METHODOLOGY

We have selected 48 galaxies from SPARC which have an important contribution of DM in the rotation curve

in order to study, from the non-parametric and parametric point of view, the seven theoretical models that we have pointed out before. This section reviews how we perform the estimation of best fit parameters as well as the statistical tools used to perform the model selection.

Regarding the parametric approach, which focus on estimating the model parameters, we use a fitting code to minimize the reduced χ_{red}^2 function,

$$\chi_{red}^2 = \frac{1}{N_d - N_p} \sum_{i=1}^N \frac{(V_{obs}(r_i) - V_{model}(r_i, \hat{\theta}))^2}{\delta V_{obs}^2(r_i)}, \quad (4)$$

where V_{obs} and δV_{obs} are the observed galaxy velocity rotation curve and its uncertainty at the observed radial distance r_i , $\hat{\theta}$ are the N_p fitting parameters of every model studied and N_d is the total number of data. Remember that $\chi_{red}^2 \sim 1$ is desirable for a good fit[36].

We also compute the P -value (χ^2 test) which gives us an indicator between the compatibility of the distribution data and the fitting model. If $P > 0.95$ this value indicates that we have a ($> 95\%$) chance to find a result less close to the central data, but, if $P < 0.05$ then the data and the fitting model are incompatible and then we can reject the fitting model, but if $P > 0.05$ we can not reject the model[36].

By virtue of we are comparing models with a different number of parameters, we compute the AIC (Akaike information criterion) and the BIC (Bayesian information criterion) to do the best model selection. In these statistical methods there is a penalty, which is applied to compensate for the obligatory difference in likelihoods due to the different number of parameters [37]. That is, if we have a model M_j with a p_j parameters, then

$$AIC = -2l(\hat{\theta}_j) + 2p_j, \quad (5)$$

where $2l(\hat{\theta}_j)$ is the goodness-of-fit term and $2p_j$ is the penalty of number of parameters. On the other hand, the Bayesian information criterion is defined as

$$BIC = -2l(\hat{\theta}_j) + 2p_j \ln N_d, \quad (6)$$

where, as before, N_d is the number of data points.

The goodness-of-fit definition used in both cases is [38]

$$l(\hat{\theta}_j) = \prod_i \frac{1}{\sqrt{2\pi\delta V_{obs}^2(r_i)}} \exp(-\chi_j^2), \quad (7)$$

where χ_j^2 and $\delta V_{obs}^2(r_i)$ describe the galaxy studied, Eq. (4), and are associated to the j -model.

AIC penalizes free parameters less strongly than does the BIC. BIC has a greater penalty for larger datasets and the AIC is independent of the sample size.

On the other side, regarding the nonparametric approach, we would like to recall we are using a technique which focuses on the fitted curve such that the fitted points and their errors are estimated with respect to the whole curve rather than a particular estimate and then

the overall uncertainty is measured as how well the estimated curve fits the data.

Here, and due that Loess+Simex reconstruction has been used in an informal graphical way to assess the relationship between variables [22–25], in order to check the validity of an specific theoretical model by comparing with the nonparametric regression curve, we compute the distance between the best χ^2 fitted velocity curve and the velocity curve obtained by reconstruction and also the distance between the 1σ band from the best χ^2 fitted curve and the 1σ band from Loess+Simex one.

We define the distance (area) between curves as:

$$D = \frac{\int_{r_{min}}^{r_{max}} |V_{Loess}(r) - V_{model}(r, \hat{\theta})| dr}{A_{DATA}}, \quad (8)$$

where $V_{Loess}(r)$ is the reconstruction velocity rotation curve from the data distribution, $V_{model}(r, \hat{\theta})$ is the velocity function of each model characterized with their parameters $\hat{\theta}$. Notice we are normalizing the area between curves with A_{DATA} , which is the area enclosing the velocity rotation data, including the error bars.

For the distance (area) between 1σ bands (model and Loess+Simex) we take into account the following cases:

- If there is not overlap between bands at a given R and the Loess 1σ band is above the model 1σ band, there we compute its contribution to the distance as

$$\delta D = \frac{1}{A_{DATA}} \int_R^{R+\delta R} |V_{Loess}^L(r) - V_{model}^U(r, \hat{\theta})| dr, \quad (9)$$

where $V_{Loess}^L(r)$ is the lower curve of the Loess 1σ band and $V_{model}^U(r, \hat{\theta})$ is the upper curve of the model 1σ band. When the model 1σ band is above the Loess 1σ band, we use a similar expression.

- If there is overlap between the 1σ bands but one band is inside the other there $\delta D = 0$. In the contrary case and if $V_{Loess}^U(r) > V_{model}^U(r, \hat{\theta})$ the contribution to the distance is given by

$$\delta D = \frac{1}{A_{DATA}} \int_R^{R+\delta R} |V_{model}^U(r, \hat{\theta}) - V_{Loess}^L(r)| dr. \quad (10)$$

If $V_{model}^U(r, \hat{\theta}) > V_{Loess}^U(r)$ the contribution to the distance is given by similar expression.

V. RESULTS AND DISCUSSION

In Table I we show the statistical results for Piso, NFW, Spano and Burkert models and for the galaxy selection of the SPARC catalog where DM is dominant.

For each model we report the χ_{red}^2 , P -value, AIC, BIC, distance between the best fit velocity curve and the reconstruction with Loess+Simex (DIST), the distance between the 1σ band from the best fit and the 1σ band from Loess+Simex ($D1\sigma$). Also in columns 26–29 are shown the Best Model columns, according with the BIC value (B_{BIC}), the distance between the Loess+Simex reconstruction and the best fit curves (B_{DIST}), the distance between 1σ bands $B_{D1\sigma}$ and χ_{red}^2 value. Columns 26–28 with models ordered according to the best values allow us to establish three conditions as a criterion to accept or reject models. The ordering is as follows.

In the table we associate a number (1–4) to each model, and for column 26 and according with the best BIC (the model with the minimum value in the BIC), we write in the first place the number of the model to point out the best one. Followed by the second one that has the best BIC between the rest, and so on. We found from the comparison of the best BIC's that the success for Piso is $\sim 20.83\%$, for NFW $\sim 14.58\%$, Spano $\sim 45.83\%$ and for Burkert $\sim 18.75\%$.

In columns 27 and 28 of Table I, we show in ascending order the models (1–4) according to the distance between Loess+Simex and best fit velocity curve (B_{DIST}) and the distance between the 1σ confidence bands for Loess+Simex and best fit velocity rotation curve, ($B_{D1\sigma}$), respectively.

From this table and according with the lower BIC, the lower distance B_{DIST} and lower distance $B_{D1\sigma}$, the percentage of galaxies satisfying the three conditions, i. e., galaxies that have the best values in all the cases, is the 47.91%. From this 47.91% of the analyzed galaxies, approximately the 60.86% points out to Spano as the most favored model and for NFW $\sim 17.39\%$, for Piso we found a percentage value of $\sim 13.04\%$ and Burkert $\sim 8.69\%$.

The lower BIC and the lower distance B_{DIST} have a preference of $\sim 20.83\%$, from which a 3% favors Spano, 40% to Burkert, NFW with 20% and Piso with the percentage value of 10%.

As an additional information we show the best χ_{red}^2 , column 29 in Table I. As we mentioned before, the first number indicates the model with the lower χ_{red}^2 . It is important to mention that in this group the number of parameters of each model is the same, therefore there is a consistency between AIC and BIC definitions where the selection of the most favorable model according to the AIC has a coincidence of 100% with the selection of the best BIC (in this case the model order for each galaxy according to AIC is the same according to BIC).

As a way to illustrate the considerable differences between the models studied in this work, by taking a look of the Best Model columns of Table I (columns 26–28), we choose four galaxies where the distance between the fitting velocity curve and the nonparametric reconstructed curve (central lines and 1σ bands) is the biggest for the NFW model. Also in accord with the respective BIC results and χ_{red}^2 , the four columns of the Best Model select NFW in the last place of the number code.

In Figs. 1 and 2 we show the observed rotation curves for four galaxies and the rotation curves that result from the fitting procedure with four models, Piso, NFW, Spano and Burkert. Also shown are the curves resulting from the nonparametric Loess-Simmex procedure. The cyan bands are the nonparametric reconstruction Loess+Simex and the red colors are for the best fit curves, 1σ and 2σ error bands, respectively. For the galaxies DDO 154, IC 2574, NGC 3109 and UGC00891 (Fig. 1), and for NFW model the distance between the best fit and 1σ bands has a noticeable separation from the Loess-Simex band and in agreement with results shown in Table I. And in Fig. 2 we show that for the rotation curves NGC 0024, NGC 0247, NGC 3741 and UGC 05716, Spano and Burkert models are having the bigger distance between the 1σ confidence and the reconstruction Loess+Simex confidence bands, even the columns of the Best Model place Spano in the last place of the selection.

On the other hand, keep in mind that Loess+Simex can provide great assistance in model selection, particularly when the data are very noisy or have other features that make patterns difficult to see. Indeed, following [39], a very simple way to assess the goodness of fit of a parametric model is by determining if the nonparametric fit falls within the parametric error bars. So, if we take a look at the Fig. 1 and the respective plots for the NFW model, for all the galaxies showed there, we note as we already said that the reconstructed curve lies outside the error bands of NFW model which indicates that this model does not appear to be a good fit to these data which in turns support our results that point out NFW is not the most favored model. The same argument can apply to the other figures.

Taking as reference the NFW model, we also studied the Schive and the Fuzzy models (SNFWDC and SNFWC) to compare the quantitative distances between the best fitting and the Loess+Simex method. From this group of models we compare core, cusp and fuzzy models, where in addition, these fuzzy models have the freedom to adapt themselves to the structure of each galaxy and reproduce core or cusp models. The position of r_ϵ , Eq. (A14), can provide us the three different structures of a galaxy: Core ($r_\epsilon > r_{max}$, being r_{max} the last observed radius of the galaxy), Cusp ($r_\epsilon \sim r_{min}$ with r_{min} is the first observed radius of the galaxy) and Core+Cusp ($r_{min} < r_\epsilon < r_{max}$).

The results of the analysis of this group of models are shown in Table II. Its description is similar to Table I. The important columns are 27–30 that give the Best Model values. Columns 27–29 are used to apply our selections criterion. Also, and in order to obtain an alternative classification value for the baryonic contribution in each galaxy, we compute $\delta A_V = 100 \frac{A_{VBar}}{A_{VObs}}$, where A_{VBar} is the total area enclosed by the baryonic velocity contribution, $\sqrt{\Upsilon_{Disk} V_{Disk}^2 + V_{Gas}^2}$ and A_{VObs} , is the area under the velocity rotation curve of the observed data (in the radius range observed), see column 2 of Table II.

Here, it is important to mention that we have three galaxies where the number of observed data is the same as the number of parameters for the SNFWC model (we use the * symbol, next to the galaxy name to identify these galaxies, see Table II); in this case we are not reporting the χ_{red}^2 and the P -value, but the other statistic quantities can be calculated.

In Figs. 3 and 4 we show the observed rotation curves for four galaxies and the rotation curves that result from the fitting procedure with four models, NFW, Schive and the Fuzzy models. Also shown are the curves resulting from the nonparametric Loess-Simmex procedure. The cyan bands are the nonparametric reconstruction Loess+Simex and the red colors are for the best fit curves, 1σ and 2σ error bands, respectively.

From Table II we studied the relationship between the lower BIC and the lower value from B_{DIST} and $B_{D1\sigma}$, and we found that $\sim 33.33\%$ of galaxies satisfy the three conditions. In this case Schive has been selected with the 43.75% to be the most favored model, NFW with 31.25%, SNFWDC 18.75% and SNFWC obtained 6.25% of model selection coincidence. On the other hand, we found $\sim 14.58\%$ of galaxies fulfill the criteria of lower BIC and lower B_{DIST} from which, SNFWDC and SNFWC have $\sim 28.57\%$ for each one and NFW has $\sim 42.85\%$.

It is important to mention that even when BIC and AIC have different penalty terms, the Best AIC is compatible with $\sim 72.91\%$ of the Best BIC selection model, which give us a strong support for the Best Selection Model techniques used in this work.

According with the Best Model columns from Table II, we observe that B_{DIST} selection model is the same for the Fuzzy models (3 and 4) in 24 galaxies, and 11 galaxies where fuzzy models have the same $B_{D1\sigma}$. If we considered the cases where B_{DIST} and $B_{D1\sigma}$ have the same value for the Fuzzy models (3 and 4) we found that only 8 galaxies fulfill this condition, for example we take galaxy NGC 0247 and compare the two columns B_{DIST} and $B_{D1\sigma}$ (from the Best Model column) and we found the combination (34) in first and second place of the numerical combination of models, respectively. This is because $r_\epsilon^{(3)} \sim r_{min}$ and $r_\epsilon^{(4)} < r_{min}$, which tell us that NFW model explains the structure for the rotation curve. For the other cases, galaxies DDO 064, DDO 168, KK 98-251 we obtain $r_\epsilon^{(3)} > r_{max}$ and $r_\epsilon^{(4)} > r_{max}$, where Schive is the dominant model for the rotation curves; for UGC 05716, UGC 07399 and UGC 08490 $r_\epsilon^{(3)} < r_{min}$ and $r_\epsilon^{(4)} < r_{min}$; and for UGC 07524 $r_\epsilon^{(3)} = r_\epsilon^{(4)} = 3.378$ kpc.

Additionally, we note that Schive model has problems to fit the final data points and NFW to fit the initial data, instead Fuzzy models solve the two problems, the transition radius r_ϵ for each SNFW model is the same for 13 galaxies, while, for the other 35 galaxies we have for SNFWDC (3), $0.11 < r_\epsilon^{(3)} < 9.4$ and for SNFWC (4), $0.15 < r_\epsilon^{(4)} < 19.7$. In the cases where SNFW models are the same, we use the B_{BIC} in order to do the model

selection because considers the penalty term for the number of parameters instead of taking the $B_{D1\sigma}$ which can lead to misleading results due error propagation in the Loess+Simex technique.

From Table II and according to the three columns of the Best Model it is possible to classify the galaxies DDO 064, DDO 168, F 571-v1, KK 98-251, NGC 6789, UGC 05986 and UGC 06399 as core type, where this criterion points out to Schive as the best model.

In a similar sense we can do the cuspy selection based on the two tables, observing that Galaxies UGC 05716 and UGC 08490 point out to NFW (with the three conditions fulfilled in both cases) as the most favored model. In the other hand, UGC 02259, UGC 05918 and UGC 12732 are selected to be cuspy from Table II, NGC 0247 and NGC 3741 from Table I, satisfying again the three Best Model columns.

If we make the comparison between the two tables (seven models) for NGC 0247, NGC 3741, UGC 02259, UGC 05918 and UGC 12732 we found:

- For NGC 0247 we compare the seven models and find that B_{BIC} and B_{DIST} points out to SNFWDC (3) and $B_{D1\sigma}$ selects NFW, if we analyze the fuzzy models we found that $r_\epsilon^{(3)} = 1.31$ kpc and the minimum radius observed for this galaxy is $r_{min} = 1.08$ kpc, in this case the major contribution in fitting the velocity of the galaxy comes from NFW ($r_\epsilon^{(3)} \sim r_{min}$, Fig. 4), therefore the fuzzy model is in agreement with Loess+Simex and the other conditions to classify the galaxy as cuspy.
- For NGC 3741, NFW satisfies B_{BIC} and $B_{D1\sigma}$ and while the B_{DIST} points out to SNFWDC, but $r_\epsilon^{(3)} = 0.268$ kpc and $r_{min} = 0.23$ kpc which NFW gives the most contribution to the galaxy structure, as an additional condition, we compare the $B_{\chi_{red}^2}$ between the seven models and found that this points out to NFW, therefore, we can classify NGC 3741 as cuspy galaxy.
- For UGC 12732 we found that NFW satisfies B_{BIC} and B_{DIST} , while PISO satisfy $B_{D1\sigma}$ and the $B_{\chi_{red}^2}$ points out to SNFWDC, where $r_\epsilon^{(3)} = 0.8$ kpc and $r_{min} = 0.96$ kpc, we can conclude that this galaxy is classified to be cuspy.

The other galaxies (UGC 02259, UGC 05918) can be excluded to be cuspy because of NFW satisfies only B_{DIST} in both of them and PISO the others conditions from Best Model column.

And finally, in Fig. 3 we show four galaxies (D 631-7, DDO168, UGC 05764 and UGC 05986) with the four models (Schive, NFW, SNFWDC and SNFWC) from where, one can see that NFW has a noticeable distance between the confidence bands and from Table II, Best Model columns, we observe these galaxies have in common that NFW is in last place from the selection number

code of models. In the figure it is displayed the best fit and 2σ confidence regions. In contrast we observed in Fig. 4 (for galaxies, NGC 0024, NGC 0247, UGC 05716 and UGC 08490) that Schive has a high distance between the reconstruction and the best fit 1σ confidence bands and also, Schive takes the last place in the selection model from the columns Best Model of Table II.

VI. CONCLUSIONS

In this work we have performed a non parametric reconstruction of galactic rotation curves by using the Loess+Simex technique as a method to discern between seven different models whose main objective is to explain the DM contribution within the rotation curves of galaxies. In order to show the efficiency of Loess+Simex and to report a quantitative result we have obtained the normalized area between the reconstructed curve and the fitted rotation curve, including also the area between 1σ bands. Due to we are comparing different models with different numbers of parameters, we use AIC and BIC information criteria methods in order to assess model fit while penalizing the number of estimated parameters and at the same time give support to Loess+Simex results. Thus, to perform model selection we use three conditions as a criterion to accept or reject models:

- B_{BIC} : the best BIC value,
- B_{DIST} : the area between the reconstructed curve and the rotation curve obtained with the best fit parameters, and
- $B_{\text{D}1\sigma}$: the area between the 1σ reconstruction band and the 1σ model fitting band.

We give to each model a numerical code (1–4) which was ordered from the lowest value up to the higher one, according to any of the above requirements, indicating in the first place (1) the most preferred model by data.

Furthermore, the DM models were separated in two groups (core + cusp and core + cusp + fuzzy models), in the first group we found that $\sim 47.91\%$ of the galaxies satisfy the three conditions, where Spano is the most favored model with $\sim 60.86\%$ and the NFW model results to be the rejected one, appearing in last place according to the three conditions with the $\sim 65.21\%$. From the second group we found that Schive is satisfying the three conditions with a 43.75% , while Schive model result to be the rejected model with the 31.25% .

By performing a comparison between these three conditions we could do a Core and Cusp classification for some of the galaxies what we have worked with, obtaining DDO 064, DDO 168, F 571-v1, KK 98-251, NGC 6789, UGC 05986 and UGC 06399 as core type, by the

other hand, NGC 0247, NGC 3741, UGC 05716, UGC 08490 and UGC 12732 can be classified as cusp galaxies, in some cases when the FUZZY models were selected by one or more of the criteria used here, the transition radius it was important to make the classification, where we observed the cases when $r_\epsilon \sim r_{\text{min}}$ pointing out to NFW as the best model to explain the structure of the galaxy and making Loess+Simex technique stronger as a model selection.

Finally, we conclude that, in the study of galactic rotation curves, the non parametric Loess+Simex method in combination with standard fitting methods can be used to perform DM models selection.

ACKNOWLEDGMENTS

A.M. acknowledges support from postdoctoral grants from DGAPA-UNAM. All authors thank SNI-CONACYT for partial support. MARM acknowledges financial support from CONACyT project 283151, from “Fondo Sectorial de Investigación para la Educación”.

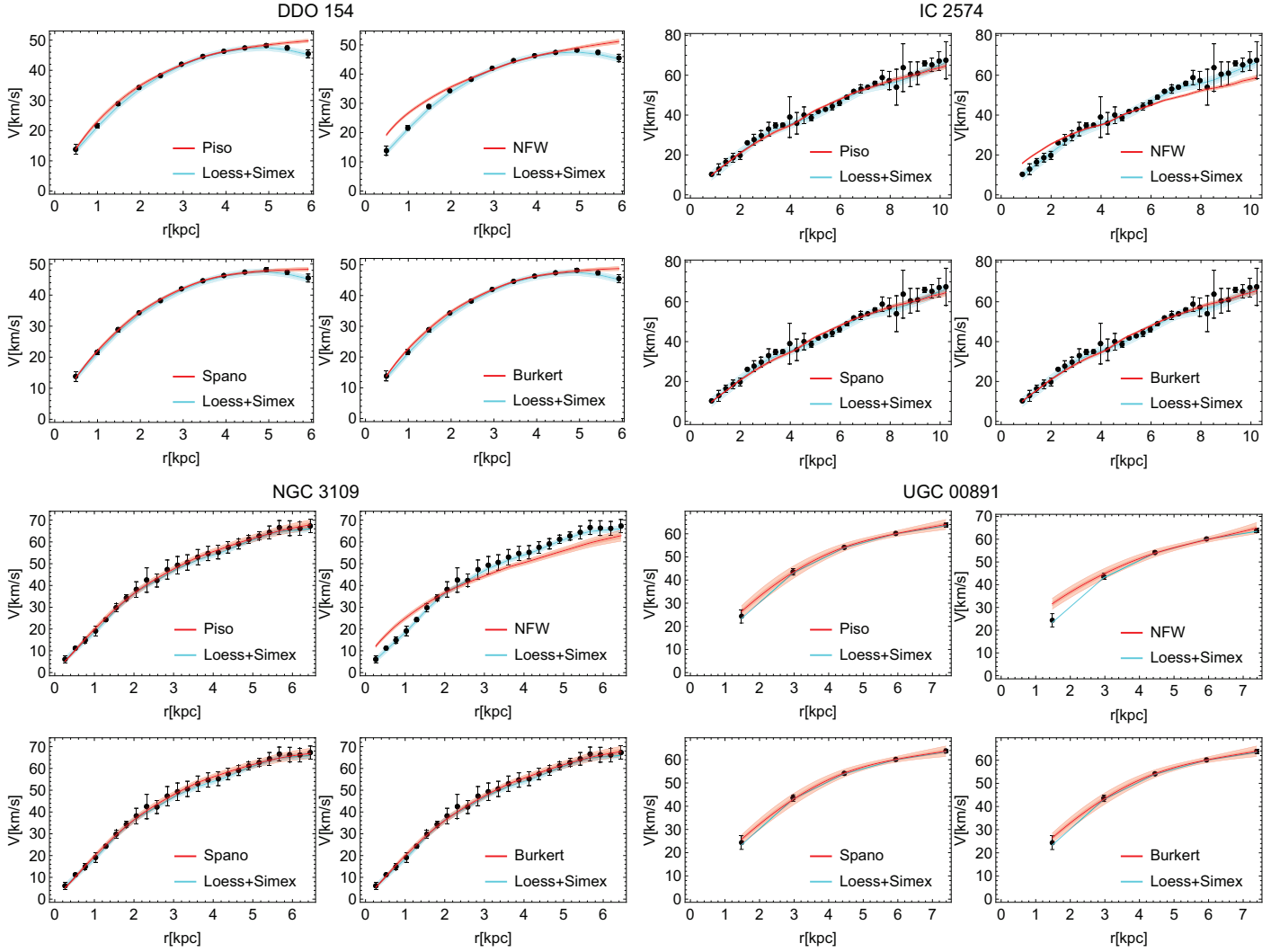


FIG. 1. Galaxies where the distance between the best fit and 1σ bands for NFW has a notable separation with the Loess+Simex band, according with the results from Table I. In the figure we show the reconstruction Loess+Simex 1 and 2σ bands in cyan color, the best fit for the four models studied in the second group including 1 and 2σ bands in red.

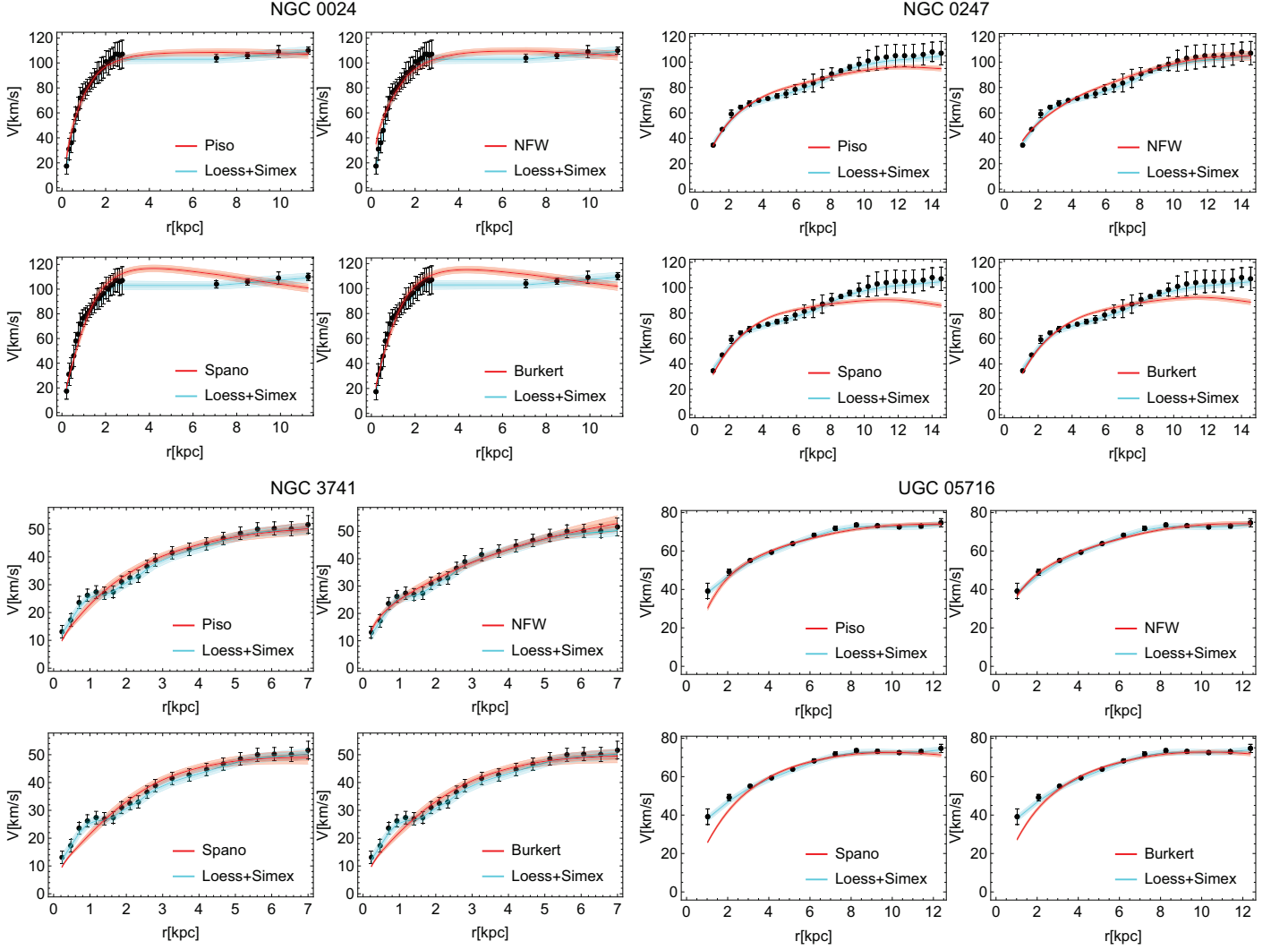


FIG. 2. Galaxies where the distance between the best fit and 1σ bands for Spano and Burkert have a notable separation with the Loess+Simex band, according with the results from Table I. In the figure we show the reconstruction Loess+Simex 1 and 2σ bands in cyan color, the best fit for the four models studied in the second group including 1 and 2σ bands in red.

SPARC Galaxies with photometry Statistics

Galaxy	δA_V	SCHIVE (1)				NFW (2)				SNFWDC (3)				SNFWC (4)				BEST MODEL												
		χ^2_{red}	P -Value	AIC	BIC	DIST	D1 σ	D2 σ	D3 σ	AIC	BIC	DIST	D1 σ	D2 σ	D3 σ	AIC	BIC	DIST	D1 σ	D2 σ	D3 σ	AIC	BIC	DIST	D1 σ	D2 σ	D3 σ			
D 512-2*	46.3	0.08	0.07	21.93	23.48	0.32	0.47	0.31	0.27	22.41	23.95	0.29	0.48	0.09	0.24	23.87	26.19	0.31	0.73	0.31	0.77	23.87	28.96	0.31	0.77	1234	2(34)1	1234	132	
D 564-8	43.9	0.04	0.003	21.82	24.98	0.26	0.26	0.91	0.55	25.30	28.47	0.22	0.36	0.04	0.009	23.75	28.50	0.25	0.35	0.26	0.31	25.82	32.15	0.26	0.31	1234	23(14)	1432	(13)42	
D 631-7	49.1	0.75	0.280	70.75	77.84	0.33	0.25	6.04	1.000	144.79	151.88	0.79	0.59	0.81	0.35	72.75	83.38	0.33	0.25	0.42	0.25	71.38	85.56	0.25	0.25	1342	4(13)2	(134)2	4132	
DDO 064	49.7	0.27	0.0066	77.97	84.52	0.22	0.16	0.56	1.124	81.42	87.98	0.30	0.16	0.30	0.0132	72.97	89.80	0.22	0.16	0.22	0.16	80.25	81.97	0.22	0.16	1234	(134)2	(1234)	1342	
DDO 154	41.9	2.00	0.971	29.33	35.27	0.38	0.26	11.77	1.000	127.05	132.99	1.86	1.55	1.34	0.73	22.05	31.40	0.43	0.47	0.43	0.47	24.49	36.37	0.43	0.49	3142	1(34)2	(134)	3412	
DDO 168	56.0	3.32	0.999	60.30	65.51	0.61	0.35	10.69	1.000	119.26	124.47	1.05	0.64	3.79	1.00	62.30	70.11	0.61	0.35	0.43	1.00	64.30	74.72	0.61	0.35	1342	(134)2	(134)2	1342	
DDO 170	49.4	6.20	1.00	60.01	64.33	0.75	0.42	2.16	0.956	35.76	40.08	0.60	0.57	1.45	0.84	32.06	38.54	0.55	0.41	0.48	0.246	28.69	37.33	0.47	0.54	4321	4321	3142	4321	
ESO 116-G012	50.0	1.42	0.86	82.96	80.79	0.34	0.33	2.35	0.9961	95.06	101.89	0.60	0.28	1.03	0.584	78.89	89.14	0.24	0.46	1.13	0.66	80.89	94.56	0.24	0.48	3142	4321	2134	3412	
ESO 444-G084	34.7	3.87	0.998	50.00	53.78	0.36	0.23	0.67	0.354	33.98	37.76	0.35	0.24	0.17	0.047	33.31	38.99	0.35	0.19	0.23	0.123	35.31	42.88	0.35	0.28	2341	(234)1	3124	3412	
F 565-V2	36.0	0.05	0.0017	44.82	48.60	0.18	0.12	0.37	0.133	46.42	50.21	0.25	0.20	0.03	0.002	46.68	52.36	0.19	0.17	0.02	0.004	48.62	56.19	0.17	0.31	1234	4132	1324	4312	
F 568-V1	46.2	0.90	0.435	126.48	134.04	0.34	0.20	3.20	1.000	163.19	170.75	0.29	0.14	0.76	0.276	125.41	136.76	0.26	0.14	0.71	0.232	125.94	141.06	0.23	0.13	1342	4321	4(23)1	4312	
F 571-V1	36.4	0.43	0.042	115.98	122.81	0.29	0.20	0.22	0.00154	113.19	120.02	0.35	0.24	0.06	2.4	10^{-6}	113.08	123.33	0.23	0.15	0.07	1.0×10^{-6}	115.08	128.74	0.23	0.13	1342	(34)12	4312	3421
F 574-1	45.7	0.09	0.006	44.73	48.52	0.23	0.24	0.32	0.008	45.90	49.68	0.26	0.27	0.01	0.0002	46.35	52.02	0.25	0.31	0.008	0.0009	48.32	55.89	0.25	0.36	1234	(34)2	1234	4312	
F 583-1	42.7	0.78	0.330	81.70	88.26	0.31	0.24	1.64	0.928	92.04	98.60	0.43	0.26	0.03	2.0	10^{-7}	74.65	84.49	0.23	0.21	0.02	7.0×10^{-8}	76.51	89.63	0.23	0.24	3142	(34)12	3(14)2	4312
F 583-4	49.1	0.28	0.0030	151.42	160.29	0.27	0.18	1.60	0.9661	181.73	190.61	0.40	0.29	0.11	6.0×10^{-8}	149.29	162.61	0.20	0.08	0.11	1.7×10^{-7}	151.28	169.03	0.20	0.11	1342	(34)12	3412	3412	
F 583-4	49.6	1.04	0.591	74.39	80.33	0.30	0.29	0.15	0.00112	65.54	71.48	0.24	0.34	0.14	0.0014	67.28	76.19	0.24	0.34	0.16	0.0039	69.28	81.15	0.25	0.41	2314	(23)41	1234	3412	
IC 2574	49.8	3.49	1.000	228.11	238.22	0.17	0.11	33.54	1.0000	1189.77	1199.88	0.49	0.36	1.31	0.8845	158.98	174.14	0.24	0.14	3.40	1.000	222.26	242.47	0.14	0.14	3142	4132	(134)2	3412	
KK 98-251	61.4	0.23	0.0022	55.39	62.23	0.25	0.09	1.82	0.9658	76.05	82.88	0.56	0.34	0.25	0.0047	57.39	67.64	0.25	0.09	0.28	0.0097	59.39	73.06	0.25	0.09	1342	(134)2	(134)2	1342	
NGC 0024	28.3	3.34	1.000	262.10	271.57	1.12	0.92	0.93	0.43	196.93	206.40	0.31	0.24	0.44	0.0057	185.14	199.34	0.36	0.24	0.21	8.8×10^{-6}	181.02	199.96	0.11	0.20	3421	4231	(4)231	4321	
NGC 0055	61.2	0.13	2.1×10^{-6}	96.56	104.73	0.22	0.12	0.97	1.000	150.50	158.68	0.45	0.35	0.13	4.5×10^{-6}	98.48	110.74	0.21	0.09	0.12	3.3×10^{-6}	100.09	116.44	0.20	0.07	1342	4312	4312	4(3)12	
NGC 0100	52.4	0.18	0.00035	114.92	123.10	0.22	0.17	0.77	0.250	126.00	134.18	0.36	0.28	0.06	6.5×10^{-9}	114.52	126.79	0.22	0.13	0.06	2.1×10^{-8}	116.49	132.85	0.21	0.11	1342	4(13)2	4312	(34)12	
NGC 0247	49.3	14.10	1.0000	458.10	467.13	0.96	0.78	1.85	0.9931	164.15	173.18	0.22	0.14	1.27	0.83	150.95	164.50	0.20	0.16	1.32	0.856	152.78	170.84	0.20	0.16	3421	(34)21	2(34)1	3421	
NGC 0300	44.7	1.80	0.9896	175.20	184.07	0.42	0.35	1.65	0.101	148.58	157.46	0.30	0.23	0.41	0.0068	144.72	158.03	0.28	0.19	0.41	0.0075	146.22	163.97	0.22	0.12	2341	4321	4321	(34)21	
NGC 3109	36.2	0.37	0.0027	104.33	113.20	0.22	0.16	8.55	1.0000	292.53	301.40	0.69	0.50	0.22	0.000047	102.62	115.93	0.17	0.1	0.23	0.000101	104.62	122.37	0.17	0.13	1342	(34)12	3412	3412	
NGC 3741	32.2	2.29	0.9989	120.87	129.05	0.51	0.30	0.34	0.0037	83.98	92.16	0.20	0.20	0.36	0.0057	85.84	98.11	0.19	0.21	0.37	0.0083	87.65	104.01	0.20	0.23	2341	(3)241	2341	2341	
NGC 6789*	40.6	0.30	0.26	24.68	26.23	0.23	0.21	2.04	0.870	28.16	29.17	0.45	0.21	0.18	0.33	26.26	28.58	0.24	0.36	1.16	0.67	40.78	50.36	0.36	0.41	4321	4132	1243	312	
UGC 00191	49.2	27.75	1.000	225.28	230.06	1.03	0.54	3.58	0.999	56.09	60.87	0.93	0.78	1.89	0.922	44.25	51.53	0.74	0.56	0.36	0.45	17.99	22.87	0.15	0.73	1342	4312	1324	3412	
UGC 00634*	43.7	1.34	0.737	19.51	21.06	1.01	1.07	3.20	0.959	23.24	24.79	1.20	0.88	0.68	0.59	19.52	21.84	0.99	1.50	0.36	0.45	17.99	22.87	0.15	0.73	1342	4312	1324	3412	
UGC 00891	47.0	0.61	0.392	15.47	17.90	0.21	0.14	3.10	0.974	22.94	25.38	0.71	0.55	0.27	0.24	16.17	19.83	0.18	0.31	0.91	0.54	38.08	46.72	0.44	0.40	2341	(23)41	2341	2341	
UGC 02259	40.7	12.50	1.00	105.48	109.80	1.20	0.74	0.71	0.355	34.69	39.01	0.37	0.31	0.85	0.484	36.69	43.17	0.37	0.34	0.36	0.45	38.08	46.72	0.44	0.40	2341	(23)41	2341	2341	
UGC 04325	43.7	1.94	0.929	48.19	52.51	0.59	0.33	2.87	0.991	53.77	58.08	0.42	0.39	0.13	0.013	39.18	45.66	0.36	0.45	0.04	0.003	40.71	49.34	0.35	0.53	3412	4321	1234	4312	
UGC 04499	54.7	0.73	0.355	44.97	49.76	0.29	0.30	1.09	0.64	47.49	52.28	0.28	0.43	0.24	0.038	43.31	50.49	0.28	0.34	0.21	0.041	44.89	54.47	0.27	0.38	1324	4(23)1	1342	4312	
UGC 05716	41.1	18.53	1.000	211.76	217.70	1.57	1.18	1.81	0.946	44.55	50.49	0.42	0.19	2.01	0.966	46.54	55.45	0.42	0.25	2.26	0.979	48.54	60.42	0.42	0.25	2341	(234)1	2(34)1	2341	
UGC 05986	47.5	0.1	0.000014	66.55	73.38	0.19	0.17	5.98	1.000	142.99	149.82	0.96	0.67	0.09	3.3×10^{-3}	42.68	49.16	0.22	0.23	0.11	0.00015	70.55	84.21	0.19	0.17	1342	(14)32	(134)2	3142	
UGC 06399	46.6	0.14	0.0048	50.11	54.89	0.21	0.21	0.66	0.292	53.73	58.52	0.33	0.27	0.04	0.0003	51.39	58.57	0.24	0.24	0.05	0.0017	53.39	62.97	0.24	0.30	1234	1(34)2	1324	3412	
UGC 06446	41.4	2.01	0.9889	118.60	125.93	0.48	0.24	0.21	0.00062	91.59	98.93	0.23	0.21	0.16	0.000190	92.66	103.66	0.21	0.23	0.13	0.000095	94.09	108.76	0.24	0.24	2341	3241	23(14)	4312	
UGC 066																														

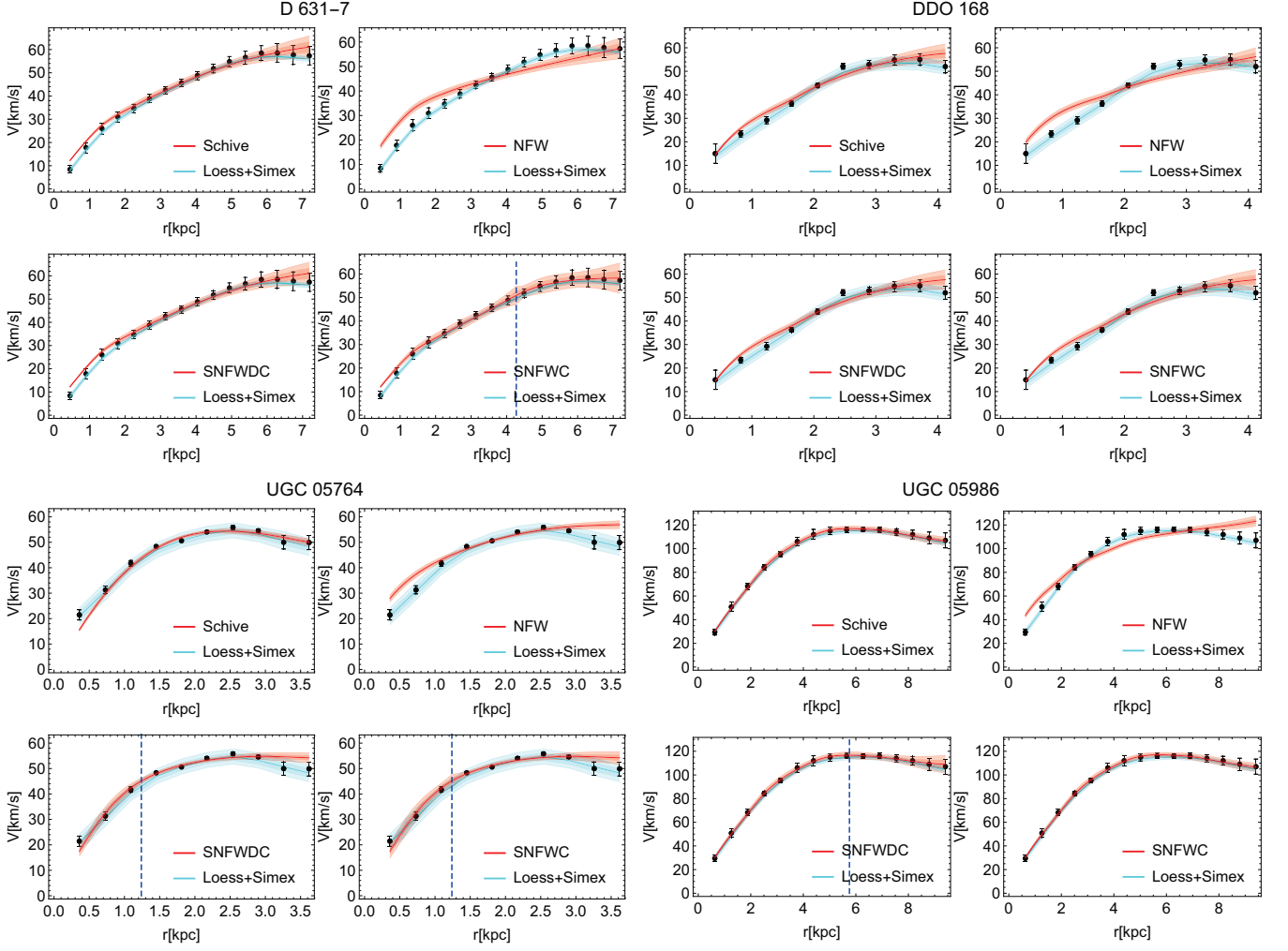


FIG. 3. Galaxies where the distance between the best fit and 1σ bands for NFW has a notable separation with the Loess+Simex band, according with the results from Table II. In the figure we show the reconstruction Loess+Simex 1 and 2σ bands in cyan color, the best fit for the four models studied in the second group including 1 and 2σ bands in red and the vertical lines correspond to r_ϵ (transition radius for the fuzzy models, Eq. (A14)).

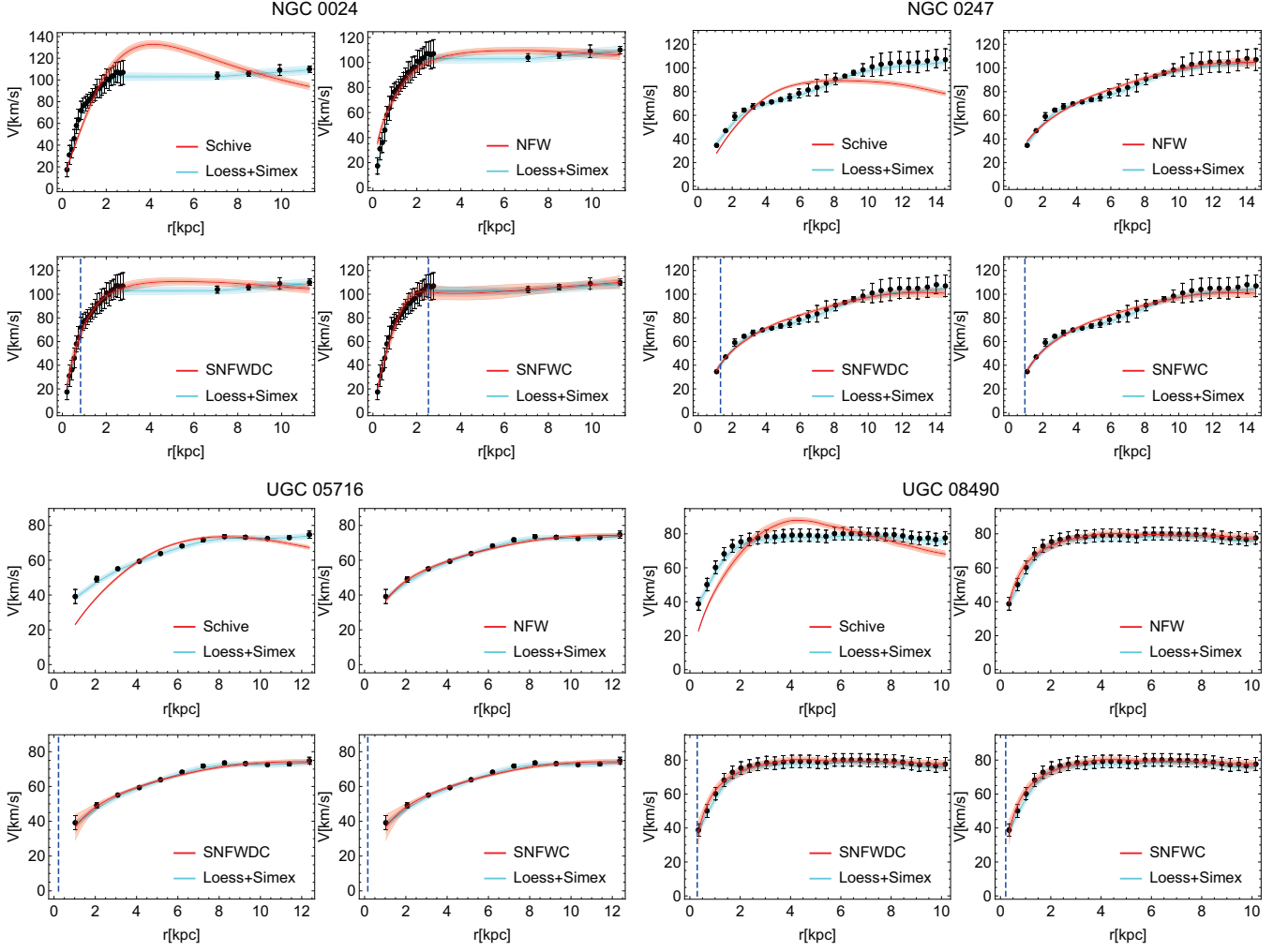


FIG. 4. Galaxies where the distance between the best fit and 1σ bands for Schive has a notable separation with the Loess+Simex band, according with the results from Table II. In the figure we show the reconstruction Loess+Simex 1 and 2σ bands in cyan color, the best fit for the four models studied in the second group including 1 and 2σ bands in red and the vertical lines correspond to r_ϵ (transition radius for the fuzzy models, Eq. (A14)).

Appendix A: CORE, CUSP AND SFDM MODELS

Here we give a brief summary of the most common models used in the literature [2–5, 8, 10]. In general a rotation curve can be described by a general expression (see [7] for more details)

$$V_{model}^2(r) = 4\pi G r_s \mu_{model} \hat{V}_{model}^2(\hat{r}), \quad (\text{A1})$$

where $\hat{V}(\hat{r})$ is a dimensionless function given by

$$\hat{V}(\hat{r}) = \sqrt{\frac{M(\hat{r})}{\hat{r}}}; \quad (\text{A2})$$

$\hat{r} = r/r_{model}$ with r_{model} being a length scale parameter for every model and $\mu_{model} = \rho_{model} r_{model}$, which is almost a constant when we fit observations but take a different value for each model [7]. The dimensionless mass at a given radius \hat{r} is given by

$$M(\hat{r}) = 4\pi \int_0^{\hat{r}} dr' r'^2 \rho_{DM}(r'). \quad (\text{A3})$$

(a) **Pseudo isothermal profile.** The DM density profile is written as [2]:

$$\rho_{PISO}(r) = \frac{\rho_p}{1 + (r/r_p)^2}. \quad (\text{A4})$$

We can write the Eq. (A1), for PISO model as

$$\hat{V}_p^2(\hat{r}_p) = \frac{\hat{r}_p - \arctan(\hat{r}_p)}{\hat{r}_p}, \quad (\text{A5})$$

where $\hat{r}_p = r/r_p$.

(b) **Navarro-Frenk-White profile.** Another interesting case (motivated by cosmological N -body simulations) is the cuspy NFW density profile which is given by [3]:

$$\rho_{NFW}(r) = \frac{\rho_n}{(r/r_n)(1 + r/r_n)^2}, \quad (\text{A6})$$

where the dimensionless velocity for this model is

$$\hat{V}_{NFW}^2(\hat{r}_n) = \frac{1}{\hat{r}_n} \ln(1 + \hat{r}_n) - \frac{1}{1 + \hat{r}_n}, \quad (\text{A7})$$

and $\hat{r}_n = r/r_n$ is defined using the scale radius r_n .

(c) **Burkert profile.** Another core density profile proposed by Burkert [4] is:

$$\rho_{Burk} = \frac{\rho_b}{(1 + r/r_b)(1 + (r/r_b)^2)}, \quad (\text{A8})$$

with the above density profile we have

$$\hat{V}_{Burk}^2(\hat{r}_b) = \frac{1}{4\hat{r}_b} (-2 \arctan(\hat{r}_b) + \ln[(1 + \hat{r}_b^2)(1 + \hat{r}_b)]). \quad (\text{A9})$$

(d) **Spano profile.** Considering the density profile in [5]

$$\rho_{Spano} = \frac{\rho_{sp}}{(1 + (r/r_{sp})^2)^{3/2}}, \quad (\text{A10})$$

we obtain a dimensionless quantity given by

$$\hat{V}_{sp}^2(\hat{r}_{sp}) = -\frac{1}{\sqrt{1 + \hat{r}_{sp}^2}} + \frac{1}{\hat{r}_{sp}} \operatorname{arcsinh}(\hat{r}_{sp}). \quad (\text{A11})$$

(e) **Schive profile.** Here we consider that DM density profile is given by WaveDM density profile[9, 10]:

$$\rho_{WDM}(r) = \frac{\rho_w}{(1 + a_w(r/r_w)^2)^8}, \quad (\text{A12})$$

where $a_w = 0.091$. Then, if we define $\hat{r}_w = r/r_w$, it is obtained

$$\hat{V}_w^2(\hat{r}_w) = \frac{1}{215040 a_w^{3/2}} \left[\frac{a_w^{1/2}}{(1 + a_w \hat{r}_w^2)^7} (-3465 + 48580 a_w \hat{r}_w^2 + 92323 a_w^2 \hat{r}_w^4 + 101376 a_w^3 \hat{r}_w^6 + 65373 a_w^4 \hat{r}_w^8 + 231000 a_w^5 \hat{r}_w^{10} + 3465 a_w^6 \hat{r}_w^{12}) - 3465 \frac{\arctan(\sqrt{a_w} \hat{r}_w)}{\hat{r}_w} \right]. \quad (\text{A13})$$

(f) **Wave+NFW (SNFW) with continuity condition in the density profile.** In this subsection we consider the DM profile motivated by simulations where the DM can be modeled with a Scalar Field [9], using the expression for density profile for the core Eq. (A12) and the Eq. (A6) for the cuspy we obtain

$$\rho_{SNFWC}(r) = \Theta(r_\epsilon - r) \rho_{WDM}(r) + \Theta(r - r_\epsilon) \rho_{NFW}(r), \quad (\text{A14})$$

with the continuity condition on the density profiles at the matching radius r_ϵ , $\rho_{WDM}(r_\epsilon) = \rho_{NFW}(r_\epsilon)$. With this condition we have four free parameters r_w , r_ϵ , r_n and ρ_w , Eqs. (A7, A13). Then we can write the velocity rotation curve as [10]

$$\hat{V}_{SNFWC}^2(\hat{r}_w, \hat{r}_\epsilon, \hat{r}_n) = \begin{cases} \hat{V}_{WDM}(\hat{r}_w) & \text{if } \hat{r}_w \leq \frac{\hat{r}_w}{\hat{r}_\epsilon}, \\ \hat{V}_{WDM}(\frac{\hat{r}_w}{\hat{r}_\epsilon}) - \hat{V}_{NFW}(\frac{\hat{r}_n}{\hat{r}_\epsilon}) + \hat{V}_{NFW}(\hat{r}_n) & \text{if } \hat{r}_w > \frac{\hat{r}_w}{\hat{r}_\epsilon} \end{cases}$$

(g) **Wave+NFW (SNFW) with continuity condition on the density profile and on its derivative.** This case was proposed in [10]. Here we consider the same density profile Eq. (A14), the continuity condition $\rho_{WDM}(r_\epsilon) = \rho_{NFW}(r_\epsilon)$ and a differentiable continuity condition at the transition radius

$r_\epsilon, \rho'_{WDM}(r_\epsilon) = \rho'_{NFW}(r_\epsilon)$. With these conditions we have only three free parameters r_w, r_ϵ and ρ_w , where

$$\begin{aligned} \hat{V}_{SNFWDC}^2(\hat{r}_w, \hat{r}_\epsilon) &= \\ &= \begin{cases} \hat{V}_{WDM}(\hat{r}_w) & \text{if } \hat{r}_w \leq \frac{\hat{r}_w}{\hat{r}_\epsilon}, \\ \hat{V}_{WDM}(\frac{\hat{r}_w}{\hat{r}_\epsilon}) - \hat{V}_{NFW}(\frac{\hat{r}_w}{\hat{r}_\epsilon}) + \hat{V}_{NFW}(\hat{r}_w) & \text{if } \hat{r}_w > \frac{\hat{r}_w}{\hat{r}_\epsilon}. \end{cases} \end{aligned}$$

-
- [1] Y. Sofue and V. Rubin, *Annu. Rev. Astron. Astrophys.* **39**, 137 (2001).
- [2] K. G. Begeman, A. H. Broeils, and R. H. Sanders, *Mon. Not. R. astr. Soc.* **294** (1991).
- [3] J. F. Navarro, C. S. Frenk, and S. D. M. White, *Astrophys. J.* **462**, 563 (1996), astro-ph/9508025.
- [4] A. Burket, *Astrophys. J. Lett.* **L25** (1995).
- [5] M. Spano, M. Marcelin, P. Amram, C. Carignan, B. Epinat, and O. Hernandez, *Mon. Not. Roy. Astron. Soc.* **383**, 297 (2008), 0710.1345.
- [6] J. Einasto, *Trudy Astrofizicheskogo Instituta Alma-Ata* **5**, 87 (1965).
- [7] M. A. Garcia-Aspeitia, J. C. Lopez-Dominguez, C. Ortiz, S. Hinojosa-Ruiz, and M. A. Rodriguez-Meza, *Rev. Mex. Fis.* **63**, 423 (2017), arXiv: 1511.06740.
- [8] S.-R. Chen, H.-Y. Schive, and T. Chiueh, *Mon. Not. Roy. Astron. Soc.* **468**, 1338 (2017), 1606.09030.
- [9] H.-Y. Schive, T. Chiueh, and T. Broadhurst, *Nature Physics* **10**, 496 (2014), 1406.6586.
- [10] T. Bernal, L. M. Fernández-Hernández, T. Matos, and M. A. Rodríguez-Meza, *Mon. Not. Roy. Soc.* **475**, 1447 (2018), arXiv: 1701.00912.
- [11] D. Hutnerer and G. Starkman, *Phys.Rev.Lett.* **90**, 031301 (2003), astro-ph/0207517.
- [12] C. Espana-Bonet and P. Ruiz-Lapuente, *Phys.Rev.D* (2005), hep-ph/0503210.
- [13] C. Bonvin, R. Durrer, and M. Kunz, *Phys.Rev.Lett.* **96**, 191302 (2006), astro-ph/0603240.
- [14] A. Shafieloo, U. Alam, V. Sahni, and A. A. Starobinsky, *Mon.Not.Roy.Astron.Soc.* **366**, 1081 (2006), astro-ph/0505329.
- [15] T. Holsclaw, U. Alam, B. Sanso, H. Lee, K. Heitmann, et al., *Phys.Rev.Lett.* **105**, 241302 (2010), 1011.3079.
- [16] J. Alberto Vazquez, M. Bridges, M. Hobson, and A. Lasenby, *JCAP* **1209**, 020 (2012), 1205.0847.
- [17] C. Bogdanos and S. Nesseris, *JCAP* **0905**, 006 (2009), 0903.2805.
- [18] W. Cleveland, *J. Am. Statist. Assoc.* **74**, 82936 (1979).
- [19] W. Cleveland and S. J. Devlin, *J. Amer. Statist. Assoc.* **83**, 596 (1988).
- [20] J. R. Cook and L. A. Stefanski, *J. Amer. Statist. Assoc.* **89**, 1314 (1994).
- [21] L. Stefanski and J. Cook, *J. Amer. Statist. Assoc.* **90**, 1247-1256 (1995).
- [22] A. Montiel, R. Lazkoz, I. Sendra, C. Escamilla-Rivera, and V. Salzano, *Phys. Rev.* **D89**, 043007 (2014), 1401.4188.
- [23] A. Rana, D. Jain, S. Mahajan, and A. Mukherjee, *JCAP* **1607**, 026 (2016), 1511.09223.
- [24] C. Escamilla-Rivera and J. C. Fabris, *Galaxies* **4**, 76 (2016), 1511.07066.
- [25] N. Rani, D. Jain, S. Mahajan, A. Mukherjee, and N. Pires, *JCAP* **1512**, 045 (2015), 1503.08543.
- [26] F. Lelli, S. S. McGaugh, and J. M. Schombert, *Astron. J.* **152**, 157 (2016), 1606.09251.
- [27] J. Schombert and S. McGaugh, *Publications of the Astronomical Society of Australia* **31**, e036 (2014).
- [28] F. Lelli, S. S. McGaugh, J. M. Schombert, and M. S. Pawlowski, *Astrophys. J.* **836**, 152 (2017), 1610.08981.
- [29] J. Fox, *Nonparametric Simple Regression: Smoothing Scatterplots*, no. 130 in *Nonparametric Simple Regression: Smoothing Scatterplots* (SAGE Publications, 2000), ISBN 9780761915850.
- [30] R. Andersen, *Annu. Rev. Sociol* **35**, 67 (2009).
- [31] *Nist/seamtech e-handbook of statistical methods* (2012), URL <http://www.itl.nist.gov/div898/handbook/>.
- [32] C. Shalizi, *Advanced Data Analysis from an Elementary Point of View* (2012), these are the notes for 36-402, *Advanced Data Analysis*, at Carnegie Mellon.
- [33] L. Wasserman, *All of Nonparametric Statistics* (Springer, New York, 2006), ISBN 0387251456.
- [34] R. Carroll, D. Ruppert, and L. Stefanski, *The Measurement Error in Nonlinear Models*, Monographs on Statistics and Applied Probability Series (Chapman and Hall, 1995), ISBN 9780412047213.
- [35] R. J. Carroll, J. D. Maca, and D. Ruppert, *Biometrika* **86**, 541 (1999).
- [36] W. Press, S. A. Teukolsky, W. T. Vetterling, and B. P. Flannery, *Numerical Recipes* (Cambridge University Press., 2007).
- [37] E. D. Feigelson and G. J. Babu, *Modern Statistical Methods for Astronomy* (Cambridge University Press, Cambridge, UK, 2012).
- [38] D. Cousineau and T. A. Allan, *Mesure et évaluation en éducation* **37**, 63 (2015).
- [39] A. Azzalini, A. W. Bowman, and W. Hardle, *Biometrika* **76**, 1 (1989), ISSN 00063444, URL <http://www.jstor.org/stable/2336363>.